Experimental support for Townsend's Reynolds number similarity hypothesis on rough walls

Karen A. Flack, Michael P. Schultz, and Thomas A. Shapiro
Mechanical Engineering Department, United States Naval Academy, Annapolis, Maryland 21402

(Received 23 July 2004; accepted 30 October 2004; published online 28 January 2005)

The Reynolds number similarity hypothesis of Townsend [*The Structure of Turbulent Shear Flow* (Cambridge University Press, Cambridge, UK, 1976)] states that the turbulence beyond a few roughness heights from the wall is independent of the surface condition. The underlying assumption is that the boundary layer thickness δ is large compared to the roughness height k. This hypothesis was tested experimentally on two types of three-dimensional rough surfaces. Boundary layer measurements were made on flat plates covered with sand grain and woven mesh roughness in a closed return water tunnel at a momentum thickness Reynolds number Re_θ of $\sim$14 000. The boundary layers on the rough walls were in the fully rough flow regime ($k_s^+ \geqslant 100$) with the ratio of the boundary layer thickness to the equivalent sand roughness height δ/k_s greater than 40. The results show that the mean velocity profiles for rough and smooth walls collapse well in velocity defect form in the overlap and outer regions of the boundary layer. The Reynolds stresses for the two rough surfaces agree well throughout most of the boundary layer and collapse with smooth wall results outside of $3k_s$. Higher moment turbulence statistics and quadrant analysis also indicate the differences in the rough wall boundary layers are confined to $y<5k_s$. The present results provide support for Townsend's Reynolds number similarity hypothesis for uniform three-dimensional roughness in flows where $\delta/k_s \geqslant 40$. [DOI: 10.1063/1.1843135]

I. INTRODUCTION

The rough wall boundary layer is of great engineering interest, including the applications of flow over ship hulls and airplanes, as well as fluid transport. Current engineering models treat roughness as a small perturbation to the smooth wall boundary layer.[1] However, if the effect of surface roughness propagates into the outer layer, the application of rough wall models that rely on smooth wall similarity scaling will yield erroneous results. Understanding the extent of this perturbation for a variety or roughness types would improve modeling and predictive capabilities.

The engineering importance of predicting the effect of wall roughness on boundary layer and pipe flows has long been identified. Much of the seminal work in this area was carried out by Nikuradse[2] and Colebrook and White.[3] Later investigations focused on the effect of roughness on turbulence structure.[4–6] An extensive review of the present knowledge of rough wall boundary layers is given by Raupach *et al.*[7] and Jiménez.[8]

The mean velocity profile in the overlap and outer regions of a turbulent boundary layer over a smooth wall is given as

$$U^+ = \frac{1}{\kappa}\ln(y^+) + C + \frac{\Pi}{\kappa}W\left(\frac{y}{\delta}\right), \tag{1}$$

where the von Karman constant $\kappa=0.41$, the smooth wall log law intercept $C=5.0$, and Π is the wake parameter. Both Clauser[9] and Hama[10] pointed out that the primary effect of surface roughness on the mean flow is to cause a downward shift in this profile. For "k-type" rough walls, the downward shift ΔU^+ called the roughness function, correlates with k^+, the roughness Reynolds number. The mean velocity profile in the overlap and outer regions of a turbulent boundary layer over a rough wall can, therefore, be stated as

$$U^+ = \frac{1}{\kappa}\ln(y^+) + C - \Delta U^+ + \frac{\Pi}{\kappa}W\left(\frac{y}{\delta}\right). \tag{2}$$

By evaluating Eqs. (1) and (2) at $y=\delta$, Hama[11] showed that ΔU^+ can be found as the difference between the smooth wall log law intercept C and the rough wall intercept $C-\Delta U^+$ at the same Re_{δ^*}. The roughness function is, therefore, found as

$$\Delta U^+ = \left(\sqrt{\frac{2}{C_f}}\right)_S - \left(\sqrt{\frac{2}{C_f}}\right)_R = \left(\frac{U_e}{U_\tau}\right)_S - \left(\frac{U_e}{U_\tau}\right)_R. \tag{3}$$

The implicit assumption in Eq. (3) is that the mean flow for both smooth S and rough R walls obeys the velocity defect law in the overlap and outer regions of the boundary layer:

$$U_e^+ - U^+ = f\left(\frac{y}{\delta}\right). \tag{4}$$

There is a great deal of experimental support for a universal velocity defect law,[7,11–14] and it is consistent with the idea of Reynolds number similarity given by Townsend[15] that turbulence outside the inner layer is unaffected by surface condition. Some prominent rough wall studies claim that changes to the mean flow do occur in the outer layer.[16,17] This is primarily observed as an increase in the strength of the wake Π, which the researchers assert is due to the higher rate of entrainment for rough walls.

There is also a large degree of similarity in the turbulent stresses for rough and smooth walls. The Reynolds number similarity hypothesis of Townsend[15] and subsequent exten-

Report Documentation Page

Form Approved
OMB No. 0704-0188

1. REPORT DATE	2. REPORT TYPE	3. DATES COVERED
JUL 2004		**00-00-2004 to 00-00-2004**

4. TITLE AND SUBTITLE	5a. CONTRACT NUMBER
Experimental support for Townsend's Reynolds number similarity hypothesis on rough walls	5b. GRANT NUMBER
	5c. PROGRAM ELEMENT NUMBER
6. AUTHOR(S)	5d. PROJECT NUMBER
	5e. TASK NUMBER
	5f. WORK UNIT NUMBER
7. PERFORMING ORGANIZATION NAME(S) AND ADDRESS(ES) **United States Naval Academy,Department of Mechanical Engineering,Annapolis,MD,21402**	8. PERFORMING ORGANIZATION REPORT NUMBER
9. SPONSORING/MONITORING AGENCY NAME(S) AND ADDRESS(ES)	10. SPONSOR/MONITOR'S ACRONYM(S)
	11. SPONSOR/MONITOR'S REPORT NUMBER(S)

12. DISTRIBUTION/AVAILABILITY STATEMENT
Approved for public release; distribution unlimited

13. SUPPLEMENTARY NOTES

14. ABSTRACT

15. SUBJECT TERMS

16. SECURITY CLASSIFICATION OF:			17. LIMITATION OF ABSTRACT	18. NUMBER OF PAGES	19a. NAME OF RESPONSIBLE PERSON
a. REPORT **unclassified**	b. ABSTRACT **unclassified**	c. THIS PAGE **unclassified**	**Same as Report (SAR)**	**9**	

sions by Perry and Chong[18] and Raupach *et al.*[7] states that the turbulent motions are independent of surface condition outside the roughness sublayer at sufficiently high Reynolds number. This implies that the turbulent stresses, normalized by the wall shear stress, are universal outside of the roughness sublayer. The dominant view at present is that the roughness sublayer extends $\approx 3k-5k$ from the wall, where k is the roughness height. The outer region has been generally thought to be unaffected by the roughness.[7,8] This is supported by a number of studies, including the work of Perry and Li[19] on expanded mesh surfaces and Acharya *et al.*[20] for machined surfaces. Andreopoulos and Bradshaw[21] present both mean and turbulence profiles for flow over one sandpaper surface. Reynolds stress results showed good collapse outside the roughness sublayer. However, effects in the triple products were noted up to $10k$ from the wall. Ligrani and Moffat[22] presented mean and turbulence results for closely packed spheres in the transitionally rough regime. For this type of roughness element, the turbulence quantities collapsed with smooth wall results outside of the roughness sublayer. Schultz and Flack[13] examined fully rough flow over closely packed spheres with and without the addition of a secondary roughness scale. Quadrant analysis and the velocity triple products indicated that the changes in the turbulence structure in the rough wall boundary layers were confined to $y<8k_s$. Schultz and Flack[12] also tested two sand grain surfaces of varying roughness heights. Their results indicate collapse of the mean velocity in defect form and collapse of the normalized Reynolds stresses profiles for both the smooth and rough surfaces in the overlap and outer regions of the boundary layer.

Other researchers have observed roughness effects well into the outer layer. The studies of Krogstad *et al.*[16] for woven mesh roughness and Keirsbulck *et al.*[17] for transverse bar roughness indicate that the wake strength of the mean velocity profile is increased. Additionally, Krogstad and Antonia[23] noted that the turbulence structure is altered in the outer layer for a woven mesh roughness. Antonia and Krogstad[14] also observed changes in the Reynolds shear stress profiles for surfaces covered with transverse rods. These studies imply the effect of surface roughness may propagate well into the outer region.

An explanation for the disparate findings is most likely due to the "strong" roughness used in the investigations where effects were observed in the outer layer. A strong roughness here is defined as a surface whose equivalent sand roughness height[2,24] k_s is a significant portion of the inner layer thickness.[13] This view is supported in the recent review article of Jiménez[8] which asserts that surfaces where $\delta/k \leqslant 40$ may exhibit roughness effects well into the outer layer, since most of the log-law region may be destroyed by the presence of the roughness. The size of the woven mesh, traverse rods, and tranverse bars used in the studies of Krogstad *et al.*,[16] Antonia and Krogstad,[14] and Keirsbulck *et al.*[17] correspond to $\delta/k_s \approx 15$, $\delta/k_s \approx 8$, and $\delta/k_s \approx 7$, respectively, while the values of δ/k in these investigations were ≈ 48, ≈ 46, and ≈ 26, respectively. In the study of Schultz and Flack[13] on uniform packed spheres, in which differences in the turbulence structure were observed out to $8k_s$, δ/k_s, and δ/k were ≈ 30. The use of k_s to define the extent of the roughness sublayer instead of k itself was proposed by Schultz and Flack[13] because it provides a common measure of the influence of the roughness on the mean flow. The difficulty with using k_s for predicting roughness effects is that it cannot be determined *a priori* from a physical measure of a generic roughness. The authors believe that δ/k_s is a more appropriate parameter than δ/k in identifying the relative strength and extent of the roughness influence on the turbulence in the boundary layer.

In the present investigation, the flow over two three-dimensional rough surfaces, sandgrain and woven mesh, will be presented. These roughness types were selected because both surfaces have been previously studied[12,16] with contrasting results related to the extent of roughness effects in the boundary layer. The height of the roughness was chosen to produce fully rough turbulent boundary layers while maintaining conditions in which the boundary layer thickness is large compared to the equivalent sand roughness height ($\delta/k_s \geqslant 40$). The mean velocity, Reynolds stress profiles, higher order moments, as well as quadrant analysis for flow over these surfaces will be compared to smooth walls. Results will focus on the extent that the roughness effects penetrate the boundary layer.

II. EXPERIMENTAL FACILITIES AND METHODS

The present experiments were conducted in the closed circuit water tunnel facility at the United States Naval Academy Hydromechanics Laboratory. The test section is 40 cm $\times$ 40 cm in cross section and is 1.8 m in length, with a tunnel velocity range of 0–6.0 m/s. The current tests were run at a tunnel speed of ~ 3.8 m/s ($\mathrm{Re}_x = 5.1 \times 10^6$). Further details of the water tunnel facility are given in Schultz and Flack.[12,13] Three surfaces are tested in this study. One is a smooth cast acrylic surface. The other two are rough surfaces; one covered with 80 grit wet/dry sandpaper and the other with woven mesh (center line spacing = 1.0 mm, wire diameter = 0.16 mm). The maximum peak to trough roughness heights k are 0.69 mm and 0.32 mm, for the sandpaper and mesh surfaces, respectively. The test specimens were inserted into a flat plate test fixture mounted horizontally in the tunnel. The test fixture is the same as that used by Schultz and Flack.[12,13] The forward most 200 mm of the plate is covered with 36 grit sandpaper to trip the developing boundary layer. The use of a strip of roughness was shown by Klebanoff and Diehl[25] to provide effective boundary layer thickening and a fairly rapid return to self-similarity. The test specimen mounts flush into the test fixture and its forward edge is located immediately downstream of the trip. The flap was set at small angles to make minor adjustments to the upstream streamwise pressure gradient. A schematic of the test water tunnel test fixture is shown in Fig. 1.

The boundary layer profiles presented here were taken 1.35 m downstream of the leading edge of the test fixture. Profiles taken from 0.80 m to the measurement location confirmed that the flow had reached self-similarity. The trailing 150 mm of the flat plate fixture is a movable tail flap. This was set with the trailing edge up at $\sim 4°$ in the present ex-

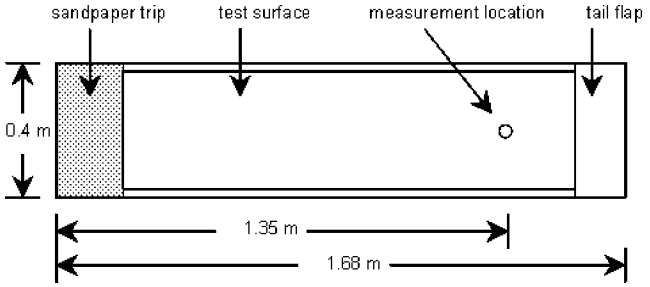

FIG. 1. Schematic of flat plate test fixture.

periments to prevent separation at the leading edge of the plate. The physical growth of the boundary layer and the inclined tail flap created a slightly favorable pressure gradient at the measurement location. The acceleration parameter K was $\sim 2.0\times 10^{-8}$ and did not vary significantly between the test surfaces.

Velocity measurements were made using a TSI FSA3500 two-component, fiber-optic laser Doppler velocimeter (LDV). The LDV used a four beam arrangement and was operated in backscatter mode. The probe volume diameter was ~ 90 μm, and its length was ~ 1.3 mm. The viscous length scale ν/u_τ varied from 5 μm for the rough walls to 7 μm for the smooth wall. The diameter of the probe volume, therefore, ranged from 13 to 18 viscous lengths in the present study. The LDV probe was mounted on a Velmex three-axis traverse unit. The traverse allowed the position of the probe to be maintained to ± 10 μm in all directions. In order to facilitate two-component, near wall measurements, the probe was tilted downwards at an angle of 4° to the horizontal and was rotated 45° about its axis. Velocity measurements were conducted in coincidence mode with 20 000 random samples per location. Doppler bursts for the two channels were required to fall within a 50 μs coincidence window or the sample was rejected.

In this study, the friction velocity u_τ for the smooth surface was found using the Clauser chart method with log-law constants $\kappa=0.41$ and $B=5.0$. For the rough walls, u_τ was obtained using a procedure based on the modified Clauser chart method given by Perry and Li.[19] Further details of the procedure are given in Refs. 12 and 26. For all the test surfaces, the total stress method was also used to verify u_τ. This method assumes a constant stress region equal to the wall shear stress exists in the overlap and inner layer of the boundary layer. If the viscous and turbulent stress contributions are added together, an expression for u_τ may be calculated as the following evaluated at the total stress plateau in the overlap and inner layer:

$$u_\tau = \left[\nu \frac{\partial U}{\partial y} - \overline{u'v'} \right]^{1/2}. \tag{5}$$

III. UNCERTAINTY ESTIMATES

Precision uncertainty estimates for the velocity measurements were made through repeatability tests using the procedure given by Moffat.[27] LDV measurements are also susceptible to a variety of bias errors including angle bias, velocity bias, and velocity gradient bias, as detailed by Edwards.[28] Fringe bias results from the inability to sample scattering particles passing through the measurement volume at large angles since several fringe crossings are needed to validate a measurement. In this experiment, the fringe bias was considered insignificant, as the beams were shifted well above a burst frequency representative of twice the freestream velocity.[28] Validation bias results from filtering too near the signal frequency and any processor biases. In general these errors are difficult to estimate and vary from system to system. No corrections were made to account for validation bias. Velocity bias results from the greater likelihood of high velocity particles moving through the measurement volume during a given sampling period. The present measurements were burst transit time weighted to correct for velocity bias, as given by Buchhave *et al.*[29] Velocity gradient bias is due to velocity variation across the measurement volume. The correction scheme of Durst *et al.*[30] was used to correct u'. The corrections to the mean velocity and the other turbulence quantities were quite small and therefore neglected. An additional bias error in the v' measurements of $\sim 2\%$ was caused by introduction of the w' component due to inclination of the LDV probe. Bias estimates were combined with the precision uncertainties to obtain the overall uncertainties for the measured quantities at 95% confidence. These were calculated using the standard methods outlined in Coleman and Steele.[31] The resulting overall uncertainty in the mean velocity is ±1%. For the turbulence quantities, $\overline{u'^2}$, $\overline{v'^2}$, and $\overline{u'v'}$ the overall uncertainties are ±2%, ±4%, and ±7%, respectively. The uncertainty in u_τ for the smooth walls using the Clauser chart method is ±3%, and the uncertainty in u_τ for the rough walls using the modified Clauser chart method was ±5%. The uncertainty in u_τ using the total stress method is ±6% for both the smooth and rough walls. The uncertainties in the boundary layer thickness δ, displacement thickness δ^*, and momentum thickness θ are ±7%, ±4%, and ±5%, respectively.

IV. RESULTS AND DISCUSSION

A. Mean flow

The experimental conditions for each of the test cases are presented in Table I. Significant increases in the physical growth of the boundary layer were noted on both rough surfaces compared to the smooth wall. The sandpaper showed increases of 21%, 58%, and 44%, while the mesh had similar increases of 18%, 57%, and 45% in δ, δ^*, and θ, respectively. As stated previously, u_τ was determined using both the total stress and Clauser chart methods. These results are also given in Table I. The agreement between the methods is within 5% in all cases. The friction velocity used for the normalization presented in this paper was obtained using the Clauser chart method due to the slightly lower uncertainty. However, it should be noted that since u_τ obtained using the total stress method was slightly less for both the smooth and rough walls, normalization based on this method would not significantly change the comparisons presented herein.

Figure 2 shows the mean velocity profiles for all three surfaces plotted in inner variables. The smooth wall log law

TABLE I. Experimental test conditions.

Surface	U_e (m/s)	Re_θ	u_τ (m/s) Total stress	u_τ (m/s) Clauser	ΔU^+	δ (mm)	δ^* (mm)	θ (mm)	$5k/\delta$	$5k_s/\delta$
Smooth	3.77	10 220	0.137	0.141	⋯	26.4	3.20	2.53	⋯	⋯
Sandpaper $k=0.69$ (mm) $k^+=134$ $k_s^+=100$	3.77	14 340	0.180	0.185	7.7	31.9	5.05	3.64	0.11	0.08
Mesh $k=0.32$ (mm) $k^+=64$ $k_s^+=138$	3.81	14 120	0.187	0.196	8.5	31.1	5.03	3.66	0.05	0.11

is shown for comparison. Both rough surfaces display a linear log region that is shifted by ΔU^+ below the smooth profile indicating an increased momentum deficit on these surfaces. The sandgrain and mesh surface produced roughness functions of $\Delta U^+=7.7$ and 8.5, respectively. It is of note that the roughness function is higher for the mesh surface at nominally the same unit Reynolds number even though the roughness height k is less than half that of the sandpaper. This clearly reinforces that the roughness height alone is not a good indicator of roughness function. Proper scaling parameters for roughness must also account for differences in parameters such as surface texture,[32] roughness density,[33] and roughness slope.[34] It was demonstrated by Furuya and Fujita[35] that not only the roughness height but also the pitch to diameter ratio is an important parameter in determining ΔU^+ on woven mesh roughness. At present, however, there is no adequate means of predicting the effect of a generic rough surface on the mean flow (i.e., ΔU^+) from measures of the roughness profile. It seems plausible that since k is not a reliable indicator (at least among different roughness types) of the roughness effect on the mean flow, it is likely not a proper length scale to define the extent of the roughness effect on the turbulent motions (known as the roughness sublayer) either. Alternatively, the equivalent sand roughness height k_s provides a common measure of the influence of the roughness on the mean flow and is related to ΔU^+ via the following,[8,22] where B, the log-law intercept for uniform sand grain, is equal to 8.5:

$$\Delta U^+ = \frac{1}{\kappa}\ln(k_s^+) + C - B. \tag{6}$$

The estimated extent of the roughness sublayer ($5k_s/\delta$) is given in Table I. Values of $5k/\delta$ are also presented for comparison.

The mean velocity profiles for all test cases are presented in defect form in Fig. 3. Also shown for comparison are the results of the smooth wall direct numerical simulation (DNS) by Spalart[36] at $\mathrm{Re}_\theta=1410$. The velocity defect profiles exhibit excellent collapse in the overlap and outer regions of the boundary layer supporting the notion of a universal defect profile for rough and smooth walls, as proposed by Clauser[9] and Hama.[10] Similar results were also observed by Acharya *et al.*[20] for mesh and machined surface roughness and by Schultz and Flack[12,13] for a variety of roughness types. Krogstad *et al.*[16] and Keirsbulck *et al.*[17] found that the defect profiles for boundary layers over woven mesh and transverse bars, respectively, did not collapse with smooth

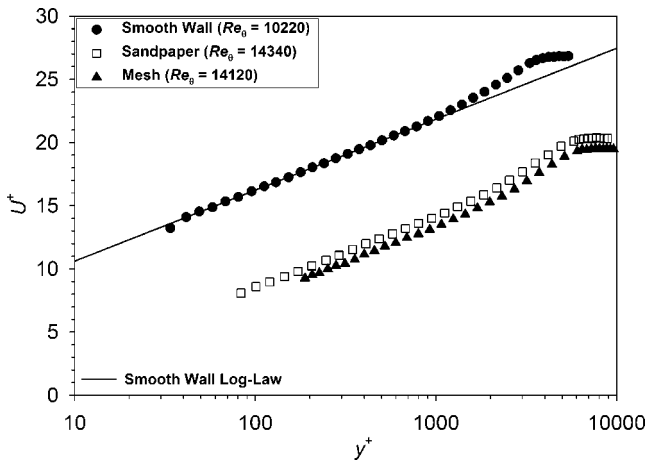

FIG. 2. Mean velocity profiles in wall coordinates (overall uncertainty in U^+: smooth wall, ±4%; rough walls, ±7%).

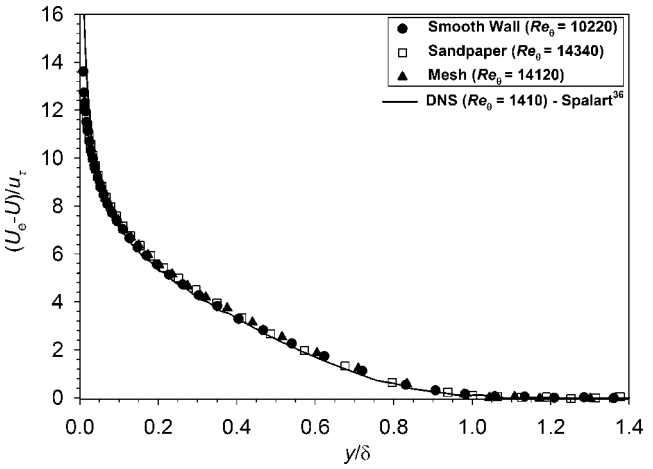

FIG. 3. Velocity defect profiles [overall uncertainty in $(U_e-U)/u_\tau$: smooth wall, ±5%; rough walls, ±7%].

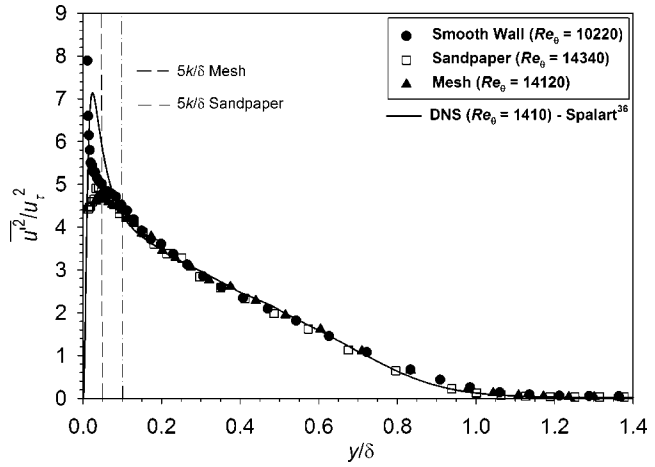

FIG. 4. Normalized streamwise Reynolds normal stress profiles (overall uncertainty in $\overline{u'^2}/u_\tau^2$: smooth wall, ±5%; rough walls, ±7%).

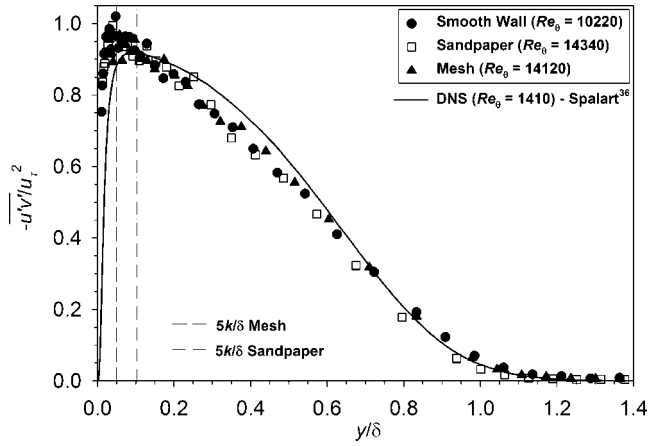

FIG. 6. Normalized Reynolds shear stress profiles (overall uncertainty in $-\overline{u'v'}/u_\tau^2$: smooth wall, ±8%; rough walls, ±10%).

wall profiles. This was due to an increase in Π for the rough walls, which presumably, resulted from the higher rate of entrainment of irrotational flow at the outer edge of the boundary layer.[16] The present authors believe the differences in results can be attributed to the strong roughness used in the studies of Krogstad *et al.*[16] and Keirsbulck *et al.*[17] In both, the ratio of the boundary layer thickness to the equivalent sand roughness height δ/k_s for the rough wall flows was $\leqslant 15$.

B. Reynolds stresses and quadrant analysis

The normalized Reynolds stress profiles ($\overline{u'^2}/u_\tau^2$, $\overline{v'^2}/u_\tau^2$, and $-\overline{u'v'}/u_\tau^2$) for the test surfaces are presented in Figs. 4–6. Also shown are the results of the smooth wall DNS by Spalart[36] at $\mathrm{Re}_\theta = 1410$. The approximate extent of the roughness sublayer for the sand grain and mesh surfaces ($5k_s/\delta$) is given for reference. The streamwise Reynolds normal stresses $\overline{u'^2}/u_\tau^2$ (Fig. 4) for the smooth and rough wall show excellent agreement throughout the overlap and outer regions of the boundary layer. Near the wall ($y/\delta \leqslant 0.05$), $\overline{u'^2}/u_\tau^2$ is significantly lower on the rough walls. The region of the roughness influence corresponds to $y \leqslant 3k_s$ on both the sandpaper and the mesh surfaces. The disappearance of the near-wall peak in $\overline{u'^2}$ was shown by Ligrani and Moffat[22] to be indicative of a boundary layer in the fully rough flow regime.

The wall-normal Reynolds normal stresses $\overline{v'^2}/u_\tau^2$ (Fig. 5) also indicate good collapse in both the overlap and outer regions of the boundary layer. This result is in agreement with a number of studies.[12,13,19,22] In the present study, the agreement in $\overline{v'^2}/u_\tau^2$ is observed for $y \geqslant k_s$ for both rough surfaces. The studies of Krogstad *et al.*[16] and Keirsbulck *et al.*[17] both showed that significant increases in the wall-normal Reynolds normal stress penetrate well into the outer layer over rough walls. It should be noted that even though the present rough surfaces are in the fully rough flow regime, they are much "weaker" in that $\delta/k_s = 63$ for the sandpaper and $\delta/k_s = 45$ for the mesh, as compared to $\delta/k_s \leqslant 15$ in those studies.

The normalized Reynolds shear stress ($-\overline{u'v'}/u_\tau^2$) profiles are presented in Fig. 6. Good collapse of the profiles is again observed across almost the entire boundary layer ($y \geqslant k_s$). In order to further investigate possible differences in the flow dynamics between smooth and rough wall boundary layers, quadrant analysis[37] was carried out using the hyperbolic hole size H method of Lu and Willmarth.[38] This technique allows the contributions of ejection $Q2$ and sweep $Q4$ motions to the Reynolds shear stress to be calculated. The contribution to $\overline{u'v'}$ from a given quadrant Q can be expressed as

$$(\overline{u'v'})_Q = \lim_{T\to\infty} \frac{1}{T}\int_0^T u'v'(t) I_Q(t)\,dt, \tag{7}$$

where $I_Q(t)$ is a trigger function defined as

$$I_Q = \begin{cases} 1 & \text{when } |u'v'|_Q \geqslant H\sqrt{\overline{u'^2}}\sqrt{\overline{v'^2}} \\ 0 & \text{otherwise.} \end{cases} \tag{8}$$

Figure 7 shows the normalized contribution from ejection and sweep events to the Reynolds shear stress for $H=0$. The profiles of both the $Q2$ and $Q4$ contributions for the smooth and rough walls show excellent agreement across almost the entire boundary layer. All the surfaces display a nearly linear

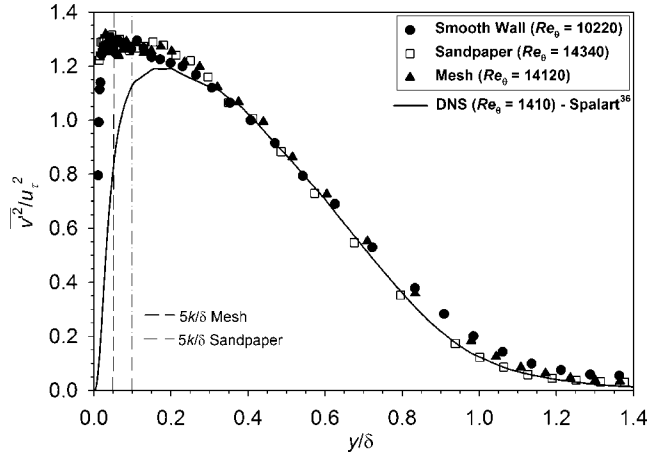

FIG. 5. Normalized wall-normal Reynolds normal stress profiles (overall uncertainty in $\overline{v'^2}/u_\tau^2$: smooth wall, ±6%; rough walls, ±8%).

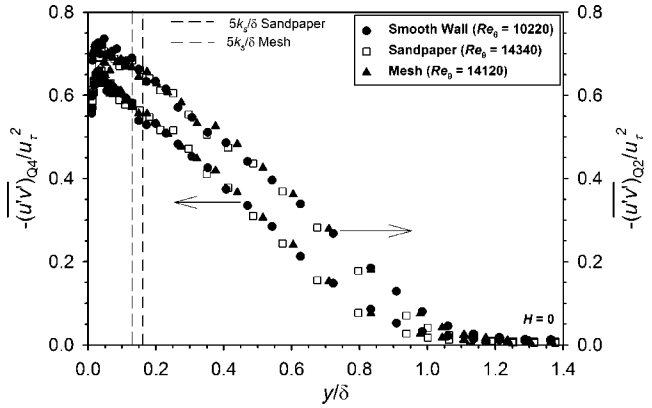

FIG. 7. Normalized Reynolds shear stress contributions from $Q2$ and $Q4$ with $H=0$ (overall uncertainty in $-(\overline{u'v'})_{Q2}/u_\tau^2$ and $-(\overline{u'v'})_{Q4}/u_\tau^2$: ±10%).

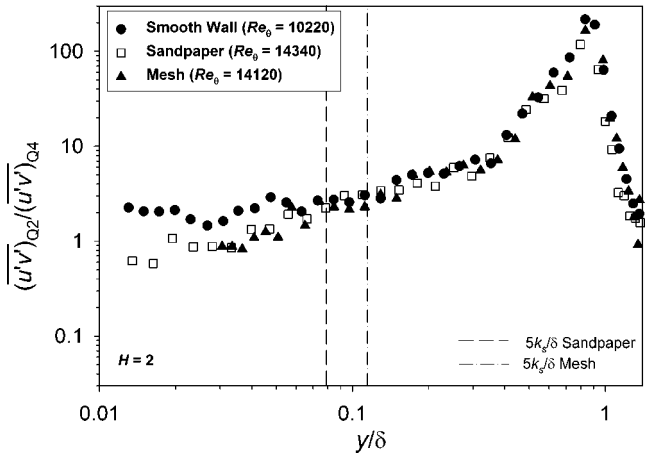

FIG. 9. Ratio of the Reynolds shear stress contributions from $Q2$ and $Q4$ with $H=2$ (overall uncertainty in $\overline{(u'v')}_{Q2}/\overline{(u'v')}_{Q4}$: ±11%).

decrease in the $Q2$ and $Q4$ Reynolds stresses in the outer layer. This indicates that roughness-induced changes to coherent turbulent structures are confined to a near-wall roughness sublayer. It is of note that ejection events dominate sweeps throughout the boundary layer on the smooth wall and for $y \geqslant 3k_s$ on the rough walls. The results of Krogstad *et al.*[16] indicate an increase in both the $Q2$ and $Q4$ contributions for rough walls that extends well into the outer layer. Schultz and Flack[13] also observed an increase in these quantities for uniform sphere roughness, but only for $y \leqslant 5k_s$. It should be noted that both of these studies were carried out on stronger roughness ($\delta/k_s \leqslant 30$) than the present investigation.

Figure 8 shows contribution to the Reynolds shear stress from strong ($H=2$) ejection and sweep events. This H corresponds to instantaneous Reynolds shear stress events larger than $5\overline{u'v'}$. The profiles of both the $Q2$ and $Q4$ contributions for the smooth and rough walls again show excellent agreement outside the near-wall region. One difference that can be discerned is an increase in strong $Q2$ events for $y/\delta \leqslant 0.05$ on the smooth wall that is absent on the rough walls. Also, strong $Q4$ events decrease on the smooth wall over the same range. This is illustrated more clearly in Fig. 9, which shows the ratio of the contributions from $Q2$ and $Q4$ for $H=2$. Near the wall, the ratio is greater than unity for the rough walls and less than unity for the smooth wall. This indicates that while strong ejection events play a larger role near a smooth wall, sweeps have a larger contribution near rough walls. This was also observed by Krogstad *et al.*[16] and is likely due to the difference in the boundary condition at $y=0$ for smooth and rough walls. On a smooth wall, $v'=0$ at $y=0$. On a rough wall, $y=0$ is located somewhere between the roughness peaks and troughs, not on the wall, so the vertical velocity fluctuations may be nonzero. The ratios of the $Q2$ to $Q4$ contributions presented in Fig. 9 show good agreement for all of the surfaces for $y > 3k_s$.

C. Velocity triple products and higher-order moments

While the present Reynolds stress results indicate there is a great deal of similarity in the turbulence on smooth and rough walls for $y > 3k_s$, higher-order turbulence moments will now be addressed. Andreopoulos and Bradshaw[21] showed that the velocity triple products provide a sensitive indicator of changes in turbulence structure due to wall condition, however, relatively few rough wall studies have presented these statistics with the exception of Antonia and Krogstad,[14] Kiersbulck *et al.*,[17] Andreopoulos and Bradshaw,[21] and Bandyopadhyay and Watson.[39] The distri-

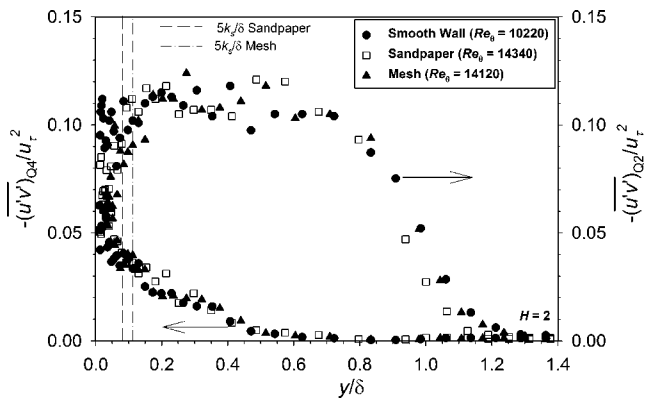

FIG. 8. Normalized Reynolds shear stress contributions from $Q2$ and $Q4$ with $H=2$ (overall uncertainty in $-(\overline{u'v'})_{Q2}/u_\tau^2$ and $-(\overline{u'v'})_{Q4}/u_\tau^2$: ±12%).

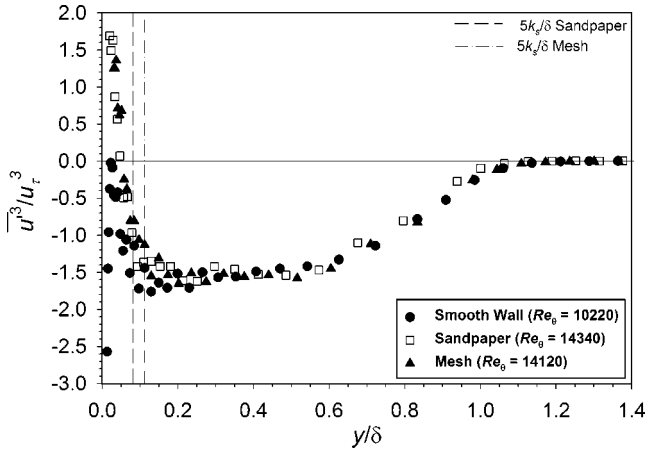

FIG. 10. Normalized velocity triple product $\overline{u'^3}/u_\tau^3$ (overall uncertainty in $\overline{u'^3}/u_\tau^3$: ±28%).

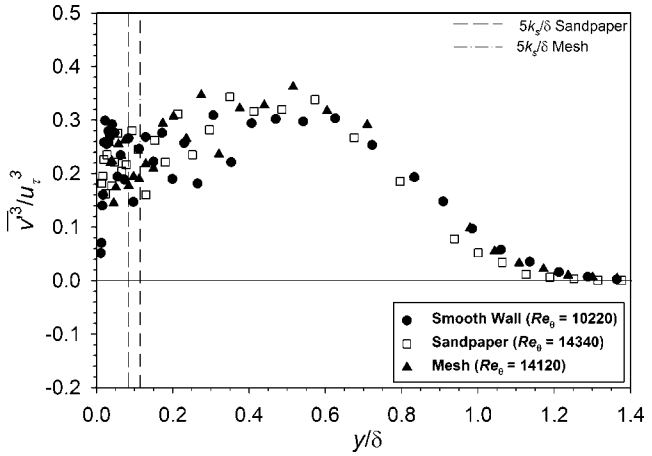

FIG. 11. Normalized velocity triple product $\overline{v'^3}/u_\tau^3$ (overall uncertainty in $\overline{v'^3}/u_\tau^3$: ±38%).

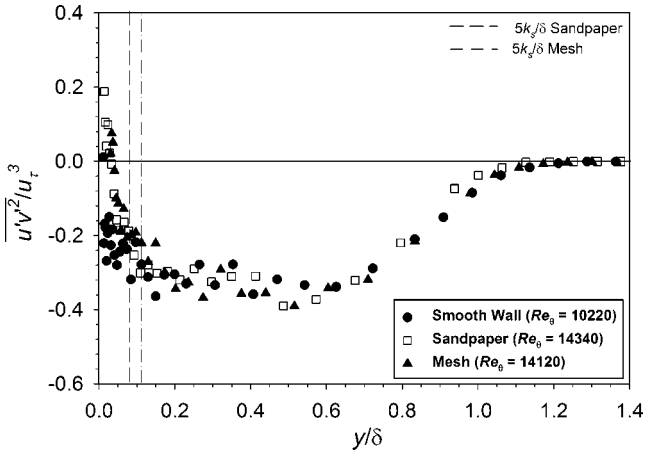

FIG. 13. Normalized velocity triple product $\overline{u'v'^2}/u_\tau^3$ (overall uncertainty in $\overline{u'v'^2}/u_\tau^3$: ±18%).

butions of the normalized velocity triple products $\overline{u'^3}/u_\tau^3$ and $\overline{u'^3}/u_\tau^3$ are presented in Figs. 10 and 11, respectively. The profiles of $\overline{u'^3}/u_\tau^3$ show good agreement between the smooth and rough walls for $y>5k_s$. Closer to the wall, some differences can be noted. The sign of $\overline{u'^3}/u_\tau^3$ is negative for the smooth wall for $y<0.05\delta$, whereas, it is positive for the rough walls. This may be due to reduced sweep events ($u'>0$) for the smooth wall than for the rough wall, which was also identified in the quadrant analysis. The profiles of $\overline{v'^3}/u_\tau^3$ also show agreement within their experimental uncertainty outside the near-wall region. This contrasts with the results of Antonia and Krogstad[14] who found large changes in this triple product for flows over transverse rod roughness. This was observed as a negative value of $\overline{v'^3}/u_\tau^3$ over a significant portion of the boundary layer indicating transport of turbulent kinetic energy towards the wall instead of away from it, as seen for a smooth wall.

The distributions of the velocity triple products $\overline{u'^2v'}/u_\tau^3$ and $\overline{u'v'^2}/u_\tau^3$ are presented in Figs. 12 and 13, respectively. The quantity $\overline{u'^2v'}/u_\tau^3$ represents the wall-normal turbulent transport of $\overline{u'^2}$. The profiles for the smooth and rough walls agree for $y>5k_s$. Much closer to the wall, there is a large reduction in $\overline{u'^2v'}/u_\tau^3$ for the rough walls. A similar trend was observed for mesh roughness by Krogstad and Antonia.[40] The gradient $\partial\overline{u'^2v'}/\partial y$ represents the turbulent diffusion of $\overline{u'^2}$ in the Reynolds stress transport equation for $\overline{u'^2}$. On the smooth wall, there is a loss in $\overline{u'^2}$ through turbulent diffusion for $0.01<y/\delta<0.025$, while there is a gain for the rough walls. The normalized turbulent flux of Reynolds shear stress $\overline{u'v'^2}/u_\tau^3$ also indicates good agreement for the smooth and rough walls over most of the boundary layer (Fig. 13). The differences in $\overline{u'v'^2}/u_\tau^3$ are confined to the near-wall region, where the wall-normal turbulent transport of Reynolds shear stress $(-\overline{u'v'})$ is toward the wall on the rough walls and away from it on the smooth wall. This difference in the near-wall transport was also observed by Andreopoulos and Bradshaw[21] and is likely due to the stronger sweep events that occur on the rough wall, as discussed previously.

The skewness factor distributions for u' and v', S_u and S_v, are shown in Figs. 14 and 15, respectively. Also shown for comparison are the smooth wall data of Antonia and Krogstad[14] at $\mathrm{Re}_0=12\,570$. There is excellent collapse of S_u for all three surfaces for $y>5k_s$ and good agreement with the smooth wall data of Antonia and Krogstad[14] outside the

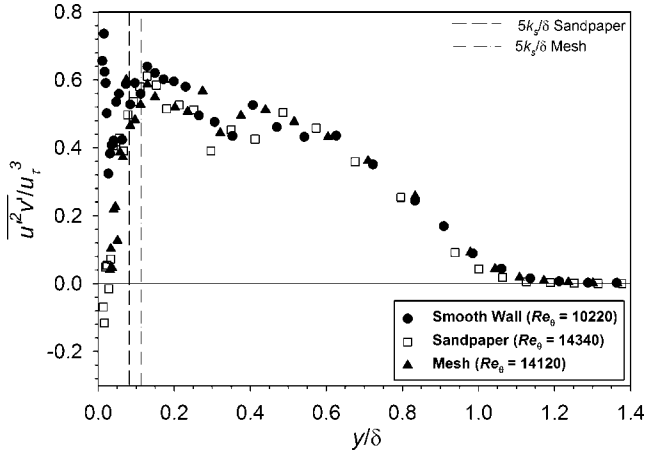

FIG. 12. Normalized velocity triple product $\overline{u'^2v'}/u_\tau^3$ (overall uncertainty in $\overline{u'^2v'}/u_\tau^3$: ±22%).

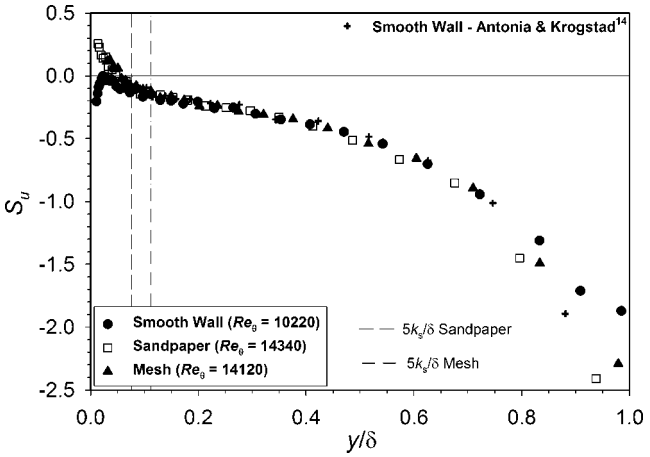

FIG. 14. Skewness factor S_u (overall uncertainty in S_u: ±25%).

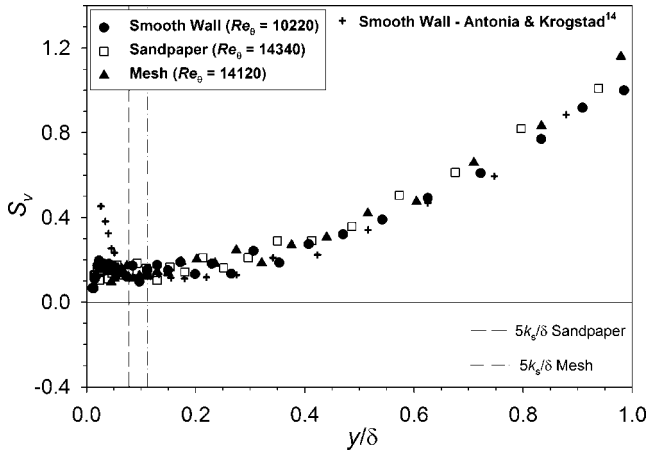

FIG. 15. Skewness factor S_v (overall uncertainty in S_v: ±35%).

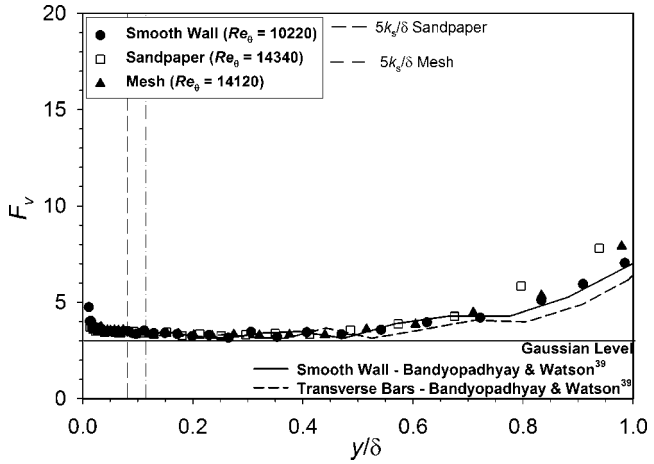

FIG. 17. Flatness factor F_v (overall uncertainty in F_v: ±6%).

roughness sublayer. Closer to the wall, the rough walls show positive skewness, while the smooth wall has negative skewness. The positive skewness near the rough walls may be due to the less strict, wall-normal boundary condition, allowing for more high momentum fluid to be swept into the near wall region. S_v shows agreement within the experimental uncertainty across the entire boundary layer (Fig. 15) and agrees well with the smooth wall data of Antonia and Krogstad[14] for $y > 5k_s$. Antonia and Krogstad[14] noted significant differences in S_v for transverse rod roughness well into the outer region of the boundary layer. The flatness factor distributions for u' and v', F_u and F_v, are shown in Figs. 16 and 17, respectively. Also included for comparison are the results of Bandyopadhyay and Watson[39] for flow over transverse bars. Both flatness factors show good collapse for smooth and rough surfaces throughout the entire boundary layer and agree reasonably well with the results of Bandyopadhyay and Watson over most of the boundary layer.

V. CONCLUSIONS

Comparisons of structure of turbulent boundary layers developing over two roughness types and a smooth wall have been made. The rough surfaces included sandpaper and woven mesh; surfaces that have previously been used to examine the concept of turbulence similarity in the outer layer.[12,16] The present results indicate that the mean velocity profiles for rough and smooth walls collapse well in velocity defect form in the overlap and outer regions of the boundary layer. The Reynolds stresses and quadrant analysis results for the two rough surfaces agree well throughout most of the boundary layer and collapse with smooth wall results for $y > 3k_s$. The velocity triple products and higher moment turbulence statistics also indicate that the differences in the rough wall boundary layers are confined to $y < 5k_s$. These results provide compelling support for Townsend's Reynolds number similarity hypothesis for uniform three-dimensional roughness in flows where the roughness is a relatively small perturbation to the smooth wall case. A survey of the literature along with the present results indicates that δ/k_s (not δ/k as Jiménez[8] recently suggested) is the proper parameter to indicate if the roughness effect on the turbulence will be strong or weak. For roughness where $\delta/k_s \geqslant 40$, significant similarity in the turbulence structure can be expected outside the roughness sublayer. In cases where $\delta/k_s < 40$, turbulence modifications may be anticipated to extend well into the outer layer. Flows with strong roughness have great practical importance. These range from engineering applications of flows through fouled heat exchanger tubes and over fouled gas turbine blades to atmospheric boundary layers in urban or forested areas. Therefore, while the concept of turbulence similarity appears applicable to many rough wall flows, further understanding and predictive capability are needed in cases where roughness effects are large and turbulence similarity fails.

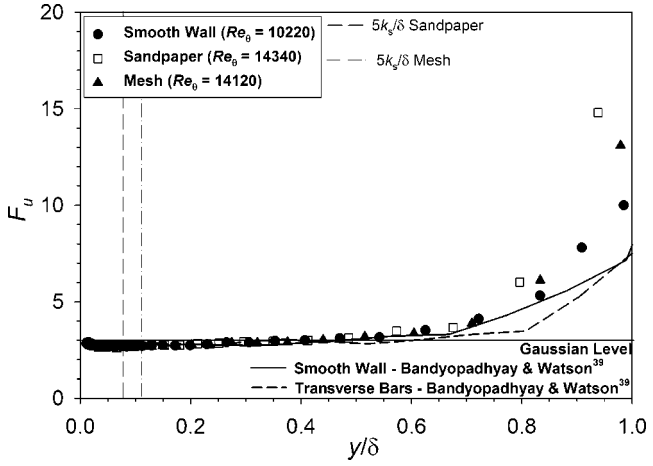

FIG. 16. Flatness factor F_u (overall uncertainty in F_u: ±3%).

[1] V. C. Patel, "Perspective: flow at high Reynolds number and over rough surfaces—Achilles heel of CFD," J. Fluids Eng. **120**, 434 (1998).
[2] J. Nikuradse, "Laws of flow in rough pipes," NACA Tech. Memo. 1292 (1933).
[3] C. F. Colebrook and C. M. White, "Experiments with fluid friction in roughened pipes," Proc. R. Soc. London **A161**, 376 (1937).
[4] A. E. Perry and P. N. Joubert, "Rough-wall turbulent boundary layers in adverse pressure gradients," J. Fluid Mech. **17**, 193 (1963).
[5] A. E. Perry, W. H. Schofield, and P. N. Joubert, "Rough-wall turbulent boundary layers," J. Fluid Mech. **37**, 383 (1969).
[6] R. A. Antonia and R. E. Luxton, "The response of a turbulent boundary

layer to a step change in surface roughness—Part 1. Smooth to rough," J. Fluid Mech. **48**, 721 (1971).
[7]M. R. Raupach, R. A. Antonia, and S. Rajagopalan, "Rough-wall turbulent boundary layers," Appl. Mech. Rev. **44**, 1 (1991).
[8]J. Jiménez, "Turbulent flow over rough walls," Annu. Rev. Fluid Mech. **36**, 173 (2004).
[9]F. H. Clauser, "Turbulent boundary layer," Adv. Appl. Mech. **4**, 1 (1956).
[10]F. R. Hama, "Boundary layer characteristics for smooth and rough surfaces," Soc. Nav. Archit. Mar. Eng., Trans. **62**, 333 (1954).
[11]P. R. Bandyopadhyay, "Rough-wall turbulent boundary layers in the transition regime," J. Fluid Mech. **180**, 231 (1987).
[12]M. P. Schultz and K. A. Flack, "Turbulent boundary layers over surfaces smoothed by sanding," J. Fluids Eng. **125**, 863 (2003).
[13]M. P. Schultz and K. A. Flack, "Outer layer similarity in fully rough turbulent boundary layers," Exp. Fluids (to be published).
[14]R. A. Antonia and P.-Å. Krogstad, "Turbulence structure in boundary layers over different types of surface roughness," Fluid Dyn. Res. **28**, 139 (2001).
[15]A. A. Townsend, *The Structure of Turbulent Shear Flow* (Cambridge University Press, Cambridge, UK, 1976).
[16]P.-Å. Krogstad, R. A. Antonia, and L. W. B. Browne, "Comparison between rough- and smooth-wall turbulent boundary layers," J. Fluid Mech. **245**, 599 (1992).
[17]L. Keirsbulck, L. Labraga, A. Mazouz, and C. Tournier, "Surface roughness effects on turbulent boundary layer structures," J. Fluids Eng. **124**, 127 (2002).
[18]A. E. Perry and M. S. Chong, "On the mechanism of wall turbulence," J. Fluid Mech. **119**, 173 (1982).
[19]A. E. Perry and J. D. Li, "Experimental support for the attached-eddy hypothesis in zero-pressure gradient turbulent boundary layers," J. Fluid Mech. **218**, 405 (1990).
[20]M. Acharya, J. Bornstein, and M. P. Escudier, "Turbulent boundary layers on rough surfaces," Exp. Fluids **4**, 33 (1986).
[21]J. Andreopoulos and P. Bradshaw, "Measurements of turbulence structure in the boundary layer on a rough surface," Boundary-Layer Meteorol. **20**, 201 (1981).
[22]P. M. Ligrani and R. J. Moffat, "Structure of transitionally rough and fully rough turbulent boundary layers," J. Fluid Mech. **162**, 69 (1986).
[23]P.-Å. Krogstad and R. A. Antonia, "Structure of turbulent boundary layers on smooth and rough walls," J. Fluid Mech. **277**, 1 (1994).
[24]H. Schlichting, *Boundary-Layer Theory*, 7th Ed. (McGraw-Hill, New York, 1979).
[25]P. S. Klebanoff and F. W. Diehl, "Some features of artificially thickened fully developed turbulent boundary layers with zero pressure gradient," NACA Tech. Memo. 2475 (1951).
[26]M. P. Schultz and A. Myers, "Comparison of three roughness function determination methods," Exp. Fluids **35**, 372 (2003).
[27]R. J. Moffat, "Describing the uncertainties in experimental results," Exp. Therm. Fluid Sci. **1**, 3 (1988).
[28]R. V. Edwards, "Report of the special panel on statistical particle bias problems in laser anemometry," J. Fluids Eng. **109**, 89 (1987).
[29]P. Buchhave, W. K. George, and J. L. Lumley, "The measurement of turbulence with the laser-Doppler anemometer," Annu. Rev. Fluid Mech. **11**, 443 (1979).
[30]F. Durst, M. Fischer, J. Jovanovic, and H. Kikura, "Methods to set up and investigate low Reynolds number, fully developed turbulent plane channel flows," J. Fluids Eng. **120**, 496 (1998).
[31]H. W. Coleman and W. G. Steele, "Engineering application of experimental uncertainty analysis," AIAA J. **33**, 1888 (1995).
[32]R. L. Townsin, D. Byrne, T. E. Svensen, and A. Milne, "Estimating the technical and economic penalties of hull and propeller roughness," Soc. Nav. Archit. Mar. Eng., Trans. **89**, 295 (1981).
[33]F. A. Dvorak, "Calculation of turbulent boundary layers on rough surfaces in pressure gradient," AIAA J. **7**, 1752 (1969).
[34]A. J. Musker, "Universal roughness functions for naturally-occurring surfaces," Trans. Can. Soc. Mech. Eng. **1**, 1 (1980).
[35]Y. Furuya and H. Fujita, "Turbulent boundary layers on a wire-screen roughness," Bull. JSME **10**, 77 (1967).
[36]P. R. Spalart, "Direct simulation of a turbulent boundary layer up to $Re_\theta = 1410$," J. Fluid Mech. **187**, 61 (1988).
[37]J. M. Wallace, H. Eckelmann, and R. S. Brodkey, "The wall region in turbulent shear flow," J. Fluid Mech. **54**, 39 (1972).
[38]S. S. Lu, and W. W. Willmarth, "Measurements of the structure of the Reynolds stress in a turbulent boundary layer," J. Fluid Mech. **60**, 481 (1973).
[39]P. R. Bandyopadhyay and R. D. Watson, "Structure of rough-wall boundary layers," Phys. Fluids **31**, 1877 (1988).
[40]P.-Å. Krogstad and R. A. Antonia, "Surface roughness effects in turbulent boundary layers," Exp. Fluids **27**, 450 (1999).